J Nondestruct Eval (2017) 36:9
DOI 10.1007/s10921-016-0386-0

Measurement and Study of Electromagnetic Emission Generated by Tensile Fracture of Polymers and Carbon Fibres

S. O. Gade[1] · **M. G. R. Sause**[2]

Received: 29 August 2016 / Accepted: 3 December 2016 / Published online: 30 December 2016

Abstract Electromagnetic emission (EME) signals generated by tensile fracture of four different types of polymers and three different carbon fibre types are presented and discussed. A suitable set-up for the detection of the electric field component of EME generated by fracture of solids is proposed. Basic theoretical considerations are made about the coupling between these field components and the capacitive sensors used to directly measure the short ranged and low frequency (kHz–MHz) electric fields emitted by the generation of free surface charges and their spatial movement as dictated by the vibrational motion of the crack walls. Special focus is put on solids with low conductivity, where the influences of the material on the emitted fields is small and the detected electric signals almost solely depend on the source dynamics and the sensor characteristics. Analysis of the influence of the acquisition circuit is presented. The discussion of the electric signals emitted by tensile fracture of carbon fibres and polymer specimens comprises the influences of the material properties on the signals as well as correlations between the signals and the crack dynamics, including the crack propagation velocities.

Keywords Electromagnetic emission · Fracture · Polymers · Carbon fibres · Crack velocity

✉ S. O. Gade
sebastian.gade@physik.uni-augsburg.de

M. G. R. Sause
markus.sause@mrm.uni-augsburg.de

[1] Institute for Physics, Experimentalphysik II, University of Augsburg, Universitätsstrasse 1, 86159 Augsburg, Germany

[2] Institute for Materials Resource Management, Mechanical Engineering, Universitätsstrasse 1, 86159 Augsburg, Germany

1 Introduction

The study of crack formation and propagation in solids is vital for the understanding of the origin and evolution of damage in structural materials. In order to monitor the occurrence of failure in a material, the acquisition of signals generated by the failure processes can be beneficial. The analysis of the measured signals may provide valuable information about their source mechanisms. This requires a sufficient understanding of the correlation between recorded signals and the generating processes. Two different kinds of signals emitted by fracture of solids are electromagnetic waves (electromagnetic emission) and acoustic waves (acoustic emission). Acoustic waves are generated by the crack dynamics and are measured as transient displacements at the materials surface. Thus, the signal is altered by the propagation from source to sensor. While the analysis of acoustic emission (AE) is a well established tool for health monitoring and the study of crack dynamics, it's complex mechanisms are still subject of research. The term electromagnetic emission (EME) comprises a wide range of emission effects. This can be electromagnetic radiation directly emitted during and after local mechanical processes, such as fracture [1,2], plastic deformation [3,4] or friction [5,6] as well as the emission of charged particles (sometimes referred to as fracto-emission [7,8]). As sources for the electromagnetic fields, the separation, displacement or movement of bound or free charges are considered. These effects have been shown for a variety of materials and source dimensions [1–3,9–11]. The emitted frequencies range from a few Hertz up to the terahertz regime, while the EME of induced or secondary effects like gas discharges between the crack sides may have even higher frequencies. Many theories and models exist for the different source mechanisms. Even for the EME accompanying frac-

ture, the mechanisms may differ for different fracture modes and materials.

Beyond the study of the source mechanism, possible applications range from a potential early warning method for earthquakes to condition monitoring. Basically, the analysis of EME can be a useful tool to study crack formation and propagation. It can provide real time information of microscopic failure, such as the duration of crack propagation or the frequencies of the crack wall vibrations [2,12,13]. In this respect, the transfer of information is almost linear. This means that the amplitude of a measured component of the electromagnetic field at the position of the sensor is proportional to certain aspects of the source like the electric dipole moment of the crack. Furthermore, the generated electromagnetic fields can be measured directly, with little to no influence of the surrounding matter and can easily be converted into voltage signals that are directly proportional to these fields. Although EME has been measured even for highly conductive materials such as metals [3], a restriction in conductivity of the investigated materials can be beneficial, e.g. with respect to the influence on the radiation pattern or the large and therefore negligible charge relaxation times. Then, EME provides a more direct observation of the crack dynamic, compared to other methods such as AE where the transfer of information suffers from influences of the propagation path like attenuation and dispersion in the material as well as effects of the specimen geometry like reflections on boundaries or even filter effects (waveguides). Also, the transfer functions of most AE sensors exhibit non-linear characteristics with respect to frequency.

As manifold the sources of EME are, as are the methods of its measurement. Depending on the frequency range and source characteristics, EME can be measured by different kinds of antennas and probes. For the frequency region discussed in this text, electric and magnetic fields are usually detected independently. Thus, sensors can basically be divided into capacitive or inductive sensors, referring to the coupling with the respective field component.

In this investigation, with a prospect of the study of failure mechanisms of carbon fibre reinforced plastics (CFRP), we focus on the EME and AE of it's components, i.e. polymers and carbon fibres, separately. Identifying and studying characteristic EME signals of these materials and analysing them in conjunction with their corresponding AE signals shall lead to a deeper understanding of the source mechanisms and provides a first basis for the examination of fracture processes in CFRP.

The present text presents a method of measuring electrical fields with frequencies up to the megahertz regime emitted by fracture of solids with low or moderate conductivity. First, a short summary of relevant theoretical considerations regarding the operational principle of the sensor system is given. Subsequently we propose a measurement set-up including electromagnetic shielding measures as well as an acquisition chain and an analysis of its transfer function. We then present results of EME and AE measurements conducted during fracture of polymer specimens and carbon fibres. A discussion of the acquired signals is made with respect to their information content. Possible correlations between the EME signals and the material properties of the tested specimens are examined. Furthermore, time dependent crack velocities are determined and discussed.

2 EME Source Description

Various theoretical models for the EME during fracture have been discussed in the past. However, a consistent model for the description of all experimental results concerning EME has yet to be proposed. Most theories presume the dynamics of charges connected to the dynamics of the fracture process to be the source of EME [12,14,15]. Some authors have pointed to the charge separation or electrification of the crack surfaces to be an important source process [6,16,17]. Both effects are also considered to occur in conjunction [18,19]. Others consider charge surface vibrational waves [2,20,21] as sources. Further effects are discussed too, e.g. polarisation effects [22,23], piezoelectric effects [24] or secondary emission effects such as light emitted by gas discharges in crack openings [10].

Also, strong directional dependencies have been observed, indicating a polar character of the sources [6,15,18,25].

In any case, the basic set of equations when dealing with electromagnetic fields in solid matter are Maxwell's equations. With restrictions in considered dimensions, time scales and the material's electric and magnetic properties this full set of equations can be severely reduced. A common approach is the classification in electroquasistatic, magnetoquasistatic and quasi-static fields [26,27].

A detailed analysis and a derivation of approximations, that can also be applied to fields generated by fracture of solids as well as the field's coupling to a sensor system, can be found in [28]. Following these approximations while considering typical time scales of crack propagation, the dimensions of the used test set-ups and the conductivities of the tested materials, the quasi-static equations prove to adequately describe the electric fields generated by fracture of polymers. Carbon fibres exhibit considerably higher conductivities and shorter crack propagation times. However, considering only characteristic time scales and set-up dimensions also allows for certain simplifications and a restriction to quasi-static fields can be justified. The specific coupling between sensor and field determines the measured field component. Electric fields couple to capacitive sensors while inductive sensors couple to the magnetic field. Both sensor types are frequently used to measure EME during fracture

tests. One important advantage of capacitive sensors over inductive sensors is the absence of strong resonances. Therefore the influence of the sensor system on the measured signals can be minimized by using capacitive sensors with a flat characteristic in the frequency region of interest.

As capacitive sensor a conductor is placed close to the crack to detect the generated field. Given an electric field distribution, analytical derivations of the potential at the sensor, depending on it's capacitance and geometry, can be conducted [29]. Furthermore, the physical quantity measured by the capacitive sensor depends on it's load conditions. If the load impedance is large compared to the source impedance the sensor mainly detects a potential, i.e. a voltage source [30]. For a fixed sensor configuration the sensor potential is then directly proportional to the electric field. For practical applications the attached load consists of multiple components as the sensor signal is usually fed into an acquisition circuit. Preferred modes of operation for such acquisition circuits are impedance matching and amplification of the voltage signal. For these purposes numerous configurations exist [31]. Depending on input impedance and capacitance of the preamplifier circuit the set-up will be characterized by a cutoff frequency. For frequencies above this cut-off frequency the system response function is absolutely flat with frequency.

If the set-up and the field distribution get more complex and simplifying assumptions for analytical approximations are not applicable anymore, numerical methods have proven to be a practical alternative approach. Fully coupled calculations of the fields and their sources and the measuring network are feasible using commercial numerical FEM tools. In principle, the whole evolution of a field generated by fracture to the recorded voltage signal can be modelled. Similar numerical analyses coupled with circuit models have been performed in related fields, e.g. for cracks as acoustic emission sources [32–34]. Such multiphysics models are also highly advantageous for improvements and optimisations of the sensor design.

3 Experimental

3.1 Sensor System

For the measurement of the electric fields generated by the fracture processes of the different materials presented in this text, we used the same basic set-up with variations in sensor geometry and amplification circuit composition. The electric fields generated by the macroscopic fracture surfaces of our polymer specimen are strong enough to be detected with little or no amplification, while the much weaker fields generated by the microscopic fracture surfaces of the carbon fibres require a considerably higher amplification.

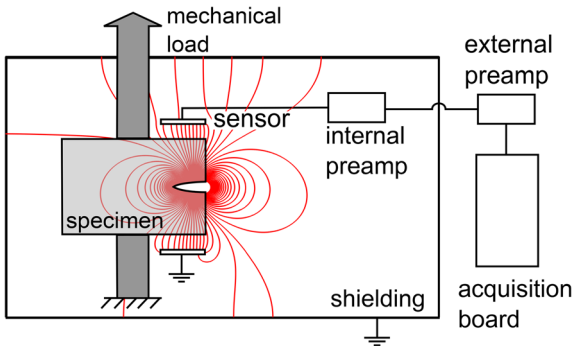

Fig. 1 **a** Schematic of proposed measurement set-up, with exemplary electric field distribution (idealized, only influenced by sensors and shielding enclosure)

A schematic of our basic set-up for the measurement of weak, fracture induced electric fields is shown in Fig. 1. The specimen is mounted on a test fixture to induce a mechanical load until fracture occurs. Copper wires of 0.5 mm diameter, placed near the specimen, are used as EME sensors (schematically depicted as small rectangular conductors in Fig. 1). The position and orientation of the sensor mainly depend on the specimen geometry and on the expected field orientation (figure 1 exemplarily shows the electric field lines generated by opposing surface charges at the crack surfaces). The specific sensor geometries for the different test set-ups are discussed in the following sections that are dedicated to the specific set-ups for the fracture tests of polymers and carbon fibres. To reduce the significant influence of the surrounding electromagnetic noise the whole set-up is encased by a shielding enclosure that also serves as ground potential. The voltage signal of the sensor is then amplified by a JFET amplifier (n-channel JFET 2SK932-22, common source circuit, with a 10 MΩ input resistor). This "internal" preamplifier is directly connected to the sensor, i.e. is also located inside the shielding enclosure. This concept was previously presented for an integrated AE sensor by Shiwa et al. [35], and is now adopted for the purpose of EME measurements. Amplifying the electric signal directly at the sensor reduces the influence of a long cable connection, e.g. the noise corruption between sensor and amplifier and the signal loss due to capacitive loading. The signal then is further amplified by a commercially available, "external" low frequency amplifier (UBBV-NF35, Aaronia AG) and recorded by a PCI-2 acquisition card (Mistras corporation, software: AEwin).

This combination of two amplification stages was only used for the fibre fracture tests. The electric fields generated by the fracture of our polymer specimen are not only much stronger than the ones generated by the fracture of the fibres, but also greatly differ in strength for the different polymers used, namely: polytetrafluorethylene (PTFE), polyether ether ketone (PEEK), polypropylene (PP) and an epoxy resin (mono-component epoxy resin system HexFlow RTM6). Therefore, two different set-ups were used for the

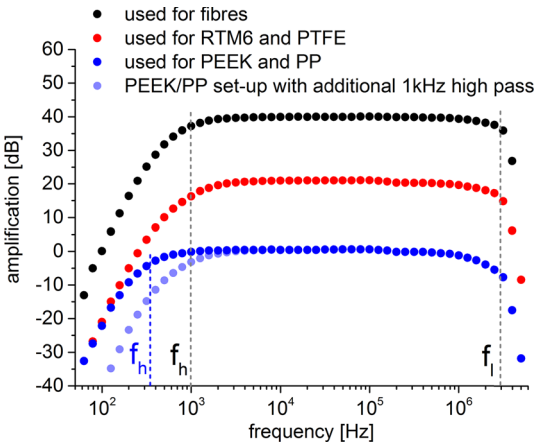

Fig. 2 Measured transfer functions of acquisition set-ups used herein, with cutoff frequencies of the low and high pass filters (Color figure online)

acquisition of these signals. For RTM6 and the PTFE specimen, only the first, "internal" preamplifier was used, leaving the total amplification at 20 dB. The fracture of the other materials, PP and PEEK, resulted in signals that exceeded the working range of this "internal" pre-amplifier. Here, we still used the JFET amplifier but decreased the input voltage by adding a 220 pF capacitor in parallel to the input resistor, thus increasing the input capacitance. This resulted in a total amplification of 0 dB.

Figure 2 shows the amplitudes of the transfer functions of the three applied amplification set-ups. While the set-ups for the fibres and the "weakly" emitting polymers (RTM6 and PTFE) only differ in amplification (black and red curves), the increase of the input capacitance for the PEEK/PP set-up (blue curve) also results in a slight shift of the high-pass cut-off frequency towards lower frequencies. Between the cut-off frequencies, which mainly reflect the bandpass characteristics of our acquisition board, the transfer functions of all three amplification set-ups are almost constant. The 1 kHz–3 MHz bandpass restriction of the used acquisition board is the major limiting factor of this set-up in terms of bandwidth. The cut-off frequencies of this bandpass correspond to specific time constants which define the upper and lower limits of measurable changes in input voltage. This results in a characteristic step response, i.e. the response of the system to an instantaneous rise in input voltage. The capability of measuring fast changes in input voltage is further limited by the maximum sample rate of 40 MHz of our acquisition card.

3.2 Properties of Tested Materials

3.2.1 Polymer Properties

To study the EME generated by tensile fracture of polymers four different polymers were chosen to be tested. The selection comprises the thermoplastic polymers PTFE, PEEK and PP as well as a thermoset polymer of cured RTM6. These polymers were selected to represent four different elastic properties to analyse the influence of the material properties on their EME.

The mechanical properties of the thermoplastic polymers were measured according to DIN EN ISO 527-1 [36], using dog-bone specimen in tensile loading (specimen shape and dimensions in accordance to DIN EN ISO 527-2 [37]). For the testing of the properties of the brittle RTM6 slightly modified dog-bone shaped specimens were used. An ARAMIS 12M digital image correlation system was used to measure the specimen deformation. Conditioning and testing was done at standard climate conditions (23 °C and 50% of relative humidity).

The densities were obtained using a helium pycnometer. The acquired results, as summarized in Table 1, are in accordance to those reported in literature.

The electric properties of the materials were obtained from measurements using a frequency response analyzer (frequency range: 1 Hz–10 MHz), an auto-balance bridge (frequency range from 20 Hz to 2 MHz), and an impedance/material analyzer (1 MHz–3 GHz). Figure 3 shows the measured values for the relative permittivity and the electric conductivity of RTM6, PP and PEEK. No measurements were performed for PTFE, since the literature values reported already indicate the highly insulating properties of the material [38]. In the context of our work, the conductivity is therefore assumed to be negligible. Due to the intrinsic dependency of the electric properties on frequency, we conducted measurements spanning the frequency range of interest for our experiments (0.1 kHz–1 MHz). While the measured values for the relative permittivity shows no significant variations in this frequency range, the values for the electric conductivity vary over a range of up to four orders in magnitude. Still, these materials can be considered low conducting for all of these frequencies.

Table 1 Material properties of polymers used

Material	Modulus (GPa)	Poisson's number	Yield str. (MPa)	Density (g/cm^3)
RTM6	2.74 ± 0.03	0.381 ± 0.006	26.2 ± 0.5	1.026 ± 0.001
PEEK	3.45 ± 0.01	0.374 ± 0.009	43.6 ± 0.5	1.301 ± 0.001
PTFE	0.72 ± 0.10	0.460 ± 0.029	4.0 ± 0.1	2.172 ± 0.003
PP	1.51 ± 0.03	0.420 ± 0.007	15.0 ± 0.3	0.919 ± 0.001

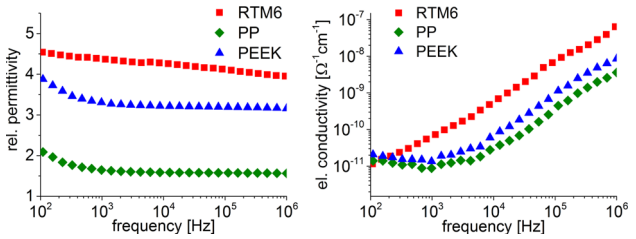

Fig. 3 Electrical properties of polymers for frequency region of interest (Color figure online)

Table 2 Mechanical properties of carbon fibres used

Material	Tens. str. (GPa)	Modulus (GPa)	Class
TohoTenax HTA40	3.0 ± 0.3	191 ± 15	HT
Sigrafil C030	4.2 ± 0.4	249 ± 9	IM
Torayca M40	3.0 ± 0.4	367 ± 5	HM-UHM

3.2.2 Carbon Fibre Properties

For the detection of EME during failure of carbon fibres tensile tests on single fibres and thin fibre bundles of less than 50 fibres were conducted. As for the polymers, different types of carbon fibres with different cross sections and material properties were used to study the influences on the EME signals. Three types of carbon fibres from different classes, a high tenacity (HT) type, a high modulus (HM) type and a intermediate modulus (IM) type, were chosen.

Single fibre tensile tests on ≥20 single fibres each were carried out to obtain the modulus and the tensile strength of the fibres types. Fibre fixation and load application was done via mechanical clamps with cushioned clamping surfaces. A displacement rate of 10 mm/min was applied, with a free fibre length of 60 mm for the modulus determination and 10 mm for the tensile strength determination. The obtained data is summarized in Table 2.

3.3 EME Test Set-Ups

3.3.1 Polymers

To induce tensile fracture of the material mode I loading of tapered double cantilever beam (TDCB) specimens was chosen. The RTM6 specimens were cured in correspondingly shaped casting molds (curing process described in detail in [18]), while the thermoplastic polymer specimens were cut from plates of 5.0–5.3 mm thickness. Pinholes, notches and side-grooves were added, the latter by using a flat end mill tilted by 45°. Figure 4b shows the specific geometry and dimensions of the specimens. Our tapered design allows for self inhibiting crack growth for the more brittle materials while preventing excessive plastic deformations at the pinholes for the more ductile materials investigated. This design also offers sufficient space for the attachment of sensors. Figure 4a shows the positions of the EME and AE sensors. For the detection of the AE signals, two acoustic, KRNBB-PC point contact sensors were attached symmetrically on both, upper and lower, halves of the specimens.

The emitted electric field is expected to show a polar character, oriented normal to the crack surfaces. Thus, the orientation of the EME sensors has to be chosen accordingly. Therefore, for the detection of the emitted directional electric fields, two wires were placed around the specimens, one wire above and one below the notch, thus effectively forming a type of capacitor with "plate" normals directed along the z-axis. A trigger based acquisition was applied for all channels. The acoustic signals, detected by the AE sensors, were amplified by 20 dB using a 2/4/6 pre-amplifier without internal bandpass filter. A 40 dB_{AE} threshold, 100/1000/300 µs as PDT/HDT/HLT and a sampling rate of 10 MS/s were set. An additional 20 kHz high pass filter was used for the measurement of the AE signals emitted during fracture of PP and PEEK. This removes part of the information content of the AE signals of these two polymers but was necessary to avoid overloading the AE amplifier.

The voltage signals at the EME sensor were amplified using a modification of the set-up as described in Sect. 3.1 (0 dB set-up for PEEK/ PP and 20 dB for RTM6/ PTFE). Here, the acquisition parameters were 500/1000/300 µs as PDT/HDT/HLT and the sampling rate was set to 5 MS/s. The thresholds were set between 42 dB_{AE} and 45 dB_{AE} (due to minor variations in noise floor amplitudes over the course of the experiments). The term dB_{AE} denotes an amplification with respect to 1 µV and will also be used for the EME detection throughout this text.

A tensile force was applied to the specimens using a test fixture as depicted in Fig. 4a and an universal testing machine (Zwick ZT 5.0). A 5 kN Xforce HP load cell was used to measure the load while it was applied displacement controlled by the testing machine. Different velocities for the displacement were chosen for different materials. This was necessary due to their different elasto-plastic behaviour. While the brittle RTM6 required a slower testing velocity of 1 mm/min to not initiate unstable crack propagation, the more ductile PP and PTFE required a higher testing velocity of 5 mm/min to initiate fracture in the first place instead of only showing plastic deformation at the notch and ductile failure of the material. For PEEK, fracture behaviour was the same for all of these velocities, so a testing velocity of 5 mm/min was applied.

Figure 5 shows representative load–displacement curves for each polymer type. The graph for RTM6 shows the expected piecewise crack propagation, with the result of multiple emission signals per specimen, i.e. one per macroscopic crack propagation event. Although exhibiting strong plastic deformation, each PTFE specimen also provided at least two measurable AE and EME signal pairs. PP and PEEK

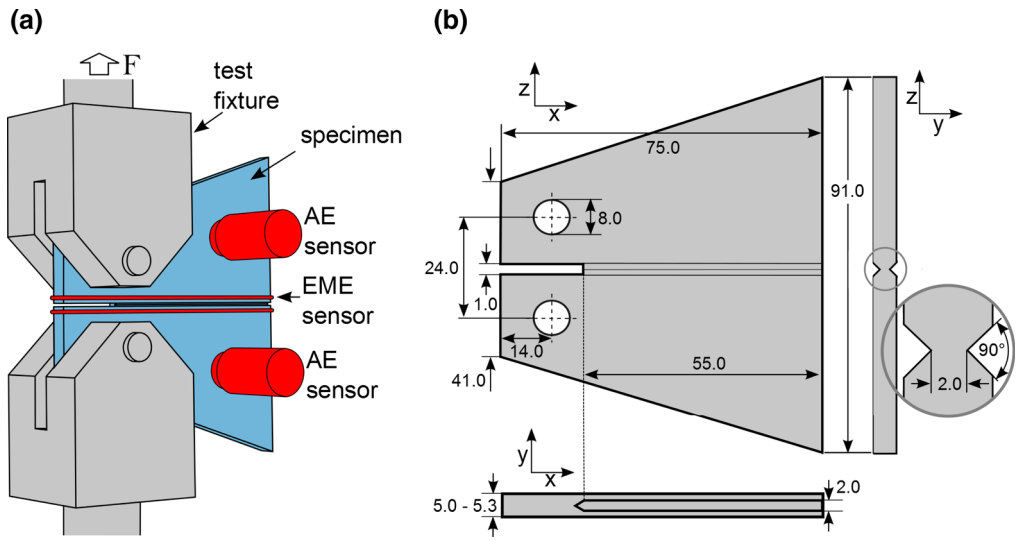

Fig. 4 **a** TDCB specimen and sensor positions. **b** specific geometry and dimensions of TDCB specimens, with detail of side-grooves

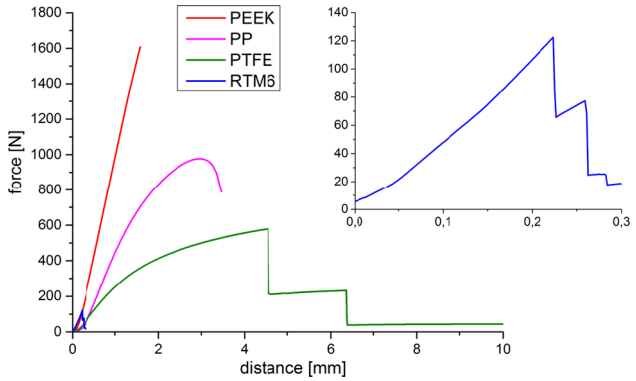

Fig. 5 Typical force–displacement curves for one representative specimen of each polymer (Color figure online)

always failed in one, unstable fracture event, only providing one strong signal per acquisition channel. Here, PP additionally showed large plastic deformation before the final failure occurred.

3.3.2 Carbon Fibres

The experimental set-up to measure EME generated by tensile fracture of carbon fibres is shown in Fig. 6. One end of a single fibre or a fibre bundle is fixed at the end of a flattened PEEK rod of 5 mm diameter using a two component epoxy adhesive. This way, the fibre is located directly at the centre of the rod diameter. The other end of the fibre is fixated at a PMMA slide, also using a drop of epoxy adhesive. The rod is connected to the testing machine (ZWICK ZT 5.0) and applies the load to the fibres. The load is applied displacement controlled with a velocity of 0.1 mm/min, and measured by a KAP-TC 5N load cell. The acoustic sensor is a KRNBB-PC point contact sensor located directly beneath the fibre

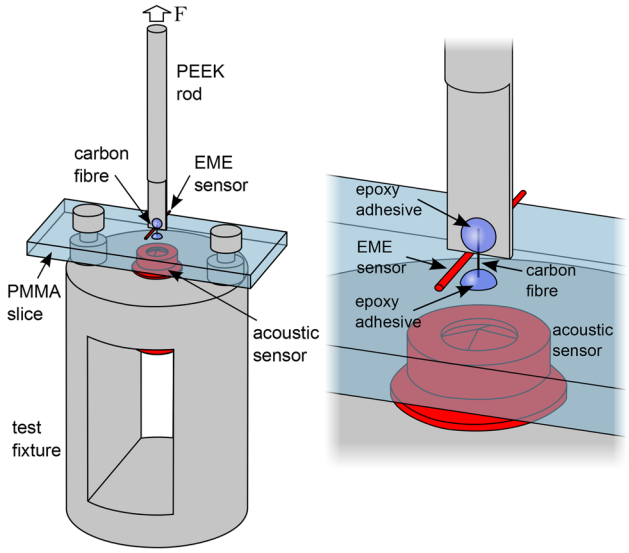

Fig. 6 Experimental set-up for the fibre tensile tests

at the bottom surface of the PMMA slide. This AE sensor placement provides the least possible influence of the propagation path, since the sensor cannot be connected directly to the fibre and has to be placed somewhere on the test fixture. The EME signals are detected by a thin copper wire near the fibres. The distance between fibres and EME sensor has to be as small as possible and was set to 1 mm. The acoustic signals were amplified by 40 dB by a 2/4/6 pre-amplifier without internal bandpass filter, while the voltage signals at the EME sensor are amplified by the two-staged amplification set-up discussed in Sect. 3.1. The thresholds were set to 40 dB_{AE} for the AE sensor and the EME sensor. Signals were recorded in synchronized mode, i.e. if a threshold is exceeded on one of the channels, signals on all channels are recorded simultaneously.

4 Results

4.1 Polymere Fracture Tests

For the sake of comparability of all EME signals, the recorded voltages signals for the PTFE and RTM6 tests were corrected for their gain to match the 0 dB amplification of the PEEK and PP tests. This reveals a considerable discrepancy in EME signal strength for the different polymers tested. Figure 7 shows the first 500 µs of the detected, unamplified EME signals for all polymers tested. For each individual polymer the EME signal strength only varies within the same order of magnitude. A comparison between the different materials shows a variation in EME signal strength of up to two orders of magnitude. The EME signals of PEEK and PP exhibit the highest signal strengths with a few hundred millivolts peak amplitudes while the RTM6 signals are by far the weakest with peak amplitudes of only some millivolts.

In [18] we presented EME signals generated by fracture of RTM6 specimen and found that the signals can be considered to consist of two mayor contributions, a slowly varying part considered to be generated by charge separation and an oscillating part considered to be generated by vibrations of the charged crack surfaces.

This consideration also applies for the EME signals presented in this text. Figure 8 shows exemplary AE and EME signals for a RTM6 specimen while Fig. 9 shows the corresponding FFT spectra. The EME signals consist of a low frequency part, which is attributed to charge separation during crack propagation, and an oscillating part, which is attributed to the vibration of the charged crack surfaces. In contrast to the signals presented in [18], with frequencies of 70–80 kHz for the oscillating part, the frequencies of the acoustic signals and the oscillating part presented here are much smaller. This is mainly attributed to the difference in fracture surface dimensions but also to specimen geometry

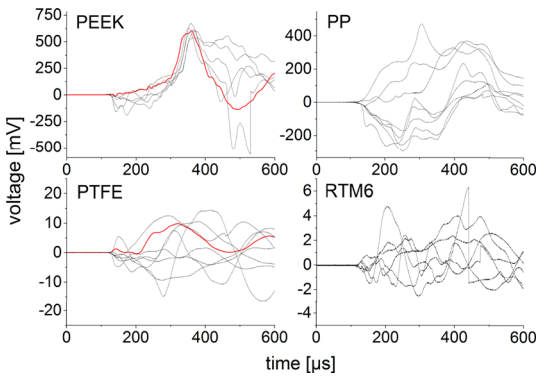

Fig. 7 Unamplified EME signals for the polymers tested. For polymers with more than one fracture event per specimen (RTM6 and PTFE) only the EME signals of the first failure are shown. Signals highlighted in *red* are used as examples in Sect. 4.1.5 (Figs. 14, 15) (Color figure online)

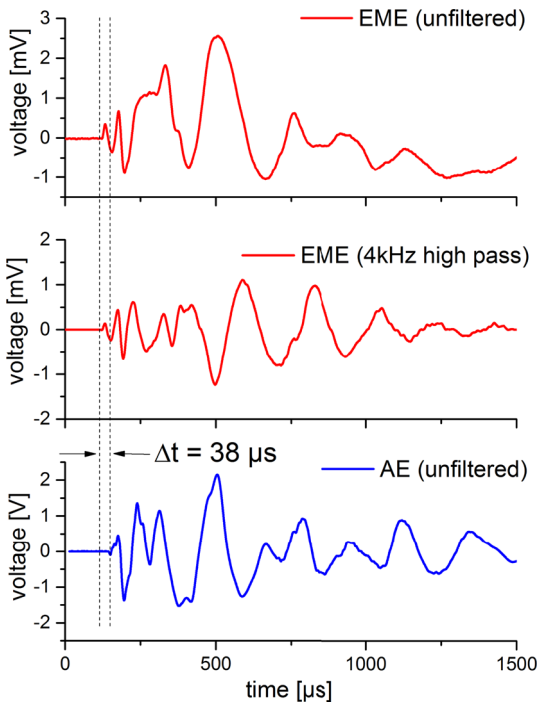

Fig. 8 Exemplary EME signal (as detected and high pass filtered) and AE signal recorded during fracture of RTM6 specimen

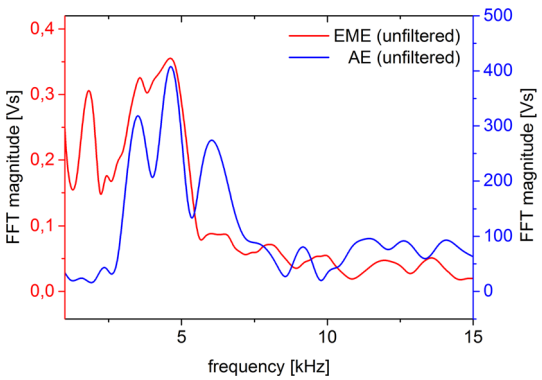

Fig. 9 FFT spectra of exemplary signal pair (as shown in Fig. 8), recorded during fracture of RTM6 specimen

and sensor placement which determine the detected wave modes.

The spectra of the electric and acoustic signals slightly differ, though both are mostly limited to frequencies below 20 kHz. Assuming the same source mechanisms for the AE and the oscillating part of the EME signals (as has been discussed in [18,19]), this difference may be a result of different transfer functions of AE and EME sensors as well as the influences of the propagation path on the AE signal. Other, superimposing effects should also be considered. The EME sensor consists of two wires that are directly attached to the polymer specimen. Thus, relative movement of the sensor wires to each other, to the grounded test fixture parts

or even relative to the charged fracture surface will result in measurable changes of the detected voltage signal. This macroscopic movement of the specimen and the attached sensors begins during crack propagation and continues after the complete failure of the specimen. Therefore, we attribute a considerable amount of the detected EME signals to this relative movement of charged materials. For this reason it proves difficult to compare the signals frequency contents. This shifts the focus to the initial, rising part of the EME signals for the following analysis. Nevertheless, this rising part's amplitude, rise time and overall characteristic is expected to contain valuable information about the fracture processes.

Figure 8 also shows the expected difference of the signal's arrival time, which is the time the acoustic signal needs to travel from the source to the AE sensor.

4.1.1 PEEK

The fracture of the PEEK specimens generates the most reproducible and strongest EME signals of the four tested polymers (see Fig. 7). The load–displacement curves for the PEEK tests (Fig. 5) indicate no significant plastic deformation before brittle fracture occurs. The fracture process seems to occur in two stages. The EME signals of the first stage exhibit lower amplitudes and slower rises when compared to the second stage and the polarities of the signals show a random character. The second stage generates a fast rise to a high EME amplitude. Surprisingly, of all detected EME signals (for all polymers) only the signals generated by this second stage of the PEEK fracture are all generated with the same polarity. No specific reason for this behaviour was found (although, assuming a random polarisation, there is also a small chance to get only one polarisation direction when testing a limited number of specimens). Figure 10 shows a microscopy image of the fracture surface of an exemplary PEEK specimen, taken after the fracture tests. Here, like for the EME signals, the two stages of crack propagation are observable by means of fractographic investigation. The first part of the crack surface is fissured and rugged. Then, the surface becomes less rough and is almost completely smooth for the rest of the crack propagation. We consequently attribute the two stages observable in the EME signals to these two different fracture processes the fracture surface indicates. The crack lengths of the two stages are approximately the same while the first stage exhibits a larger crack surface area due to the rough surface. Nevertheless, the first stage generates a weaker EME signal. This could be due to different source-sensor orientations or partial compensation of differently charged surface fragments. Or, if the fracture process differs for both stages, so could the electrification process.

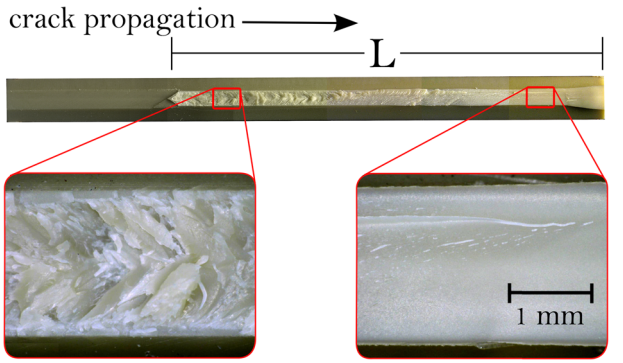

Fig. 10 Microscopy image of PEEK specimen fracture surface. *Left* First part of crack surface, rough with complex structures. *Right* Much smoother surface at the end of the crack. Full crack length for one fracture event

4.1.2 PP

The fracture of the PP specimens is preceded by large plastic deformation, as can be seen in the load–displacement curves (Fig. 5) and in the microscopy image of the fracture surface (Fig. 11). The crack starts at the notch and slowly propagates through the plastically deformed zone. Crazing processes are expected during this stage of ductile fracture. This results in a rough fracture surface that appears as white in Fig. 11. No EME or AE was recorded during this part of the crack propagation so all arising AE and EME signals are below our acquisition threshold and therefore within or below the level of the noise floor. At a certain point brittle fracture starts and complete failure of the specimen occurs. The fracture surface of this failure becomes smooth after a short and rough transition zone. The total crack length of this event is indicated as length L in Fig. 11. Strong EME and AE signals are recorded for this brittle fracture process. The EME signals are slightly weaker than the ones recorded for PEEK but this may be due to the slightly shorter crack lengths or the higher distance between the sensing wires (as a result of the plastic deformation at the beginning of crack propagation). The polarisation of the EME signals appears to be random. Nevertheless, in terms of signal strength and signal characteristic the EME signals generated by fracture of PP exhibit very good reproducibility.

4.1.3 PTFE

The fracture of the PTFE specimens was accompanied by large plastic deformation. After the initial plastic deformation, sudden fast crack growth occurs in a more brittle fashion and with measurable AE and EME. As intended by the design of the TDCB specimen geometry, and in contrast to PP and PEEK, the crack stops for the first time after a certain crack length L_1. This length in shown in Fig. 12 and is flanked

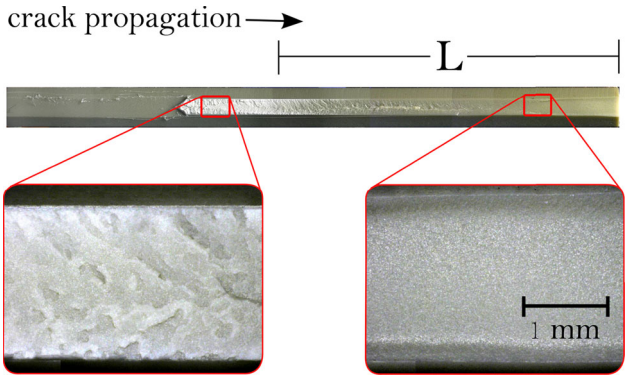

Fig. 11 Microscopy image of PP specimen fracture surface. *Left* Surface for slow crack growth after plastic deformation, no measurable EME for this part. *Right* Surface for fast crack propagation with EME, macroscopically smooth. L indicates crack length for brittle failure

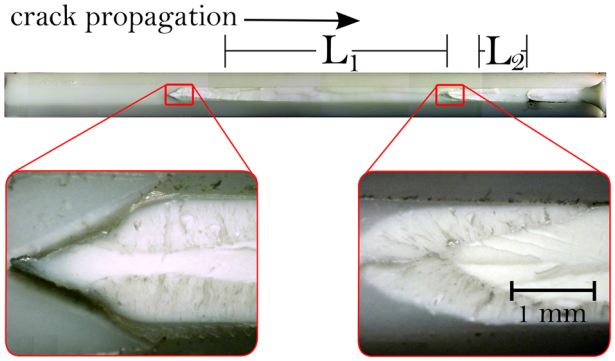

Fig. 12 Microscopy image of PTFE specimen fracture surface. *Left* Crack initiation after large plastic deformation. *Right* End of first and start of second macroscopic fracture event, with plastic deformation in between. With lengths of first two brittle fracture events

by two zones of plastic deformation and ductile fracture (white in Fig. 12). After another period of plastic deformation a second fast and brittle crack propagation phase occurs (L_2 in Fig. 12) with another pair of AE and EME signals. Although the EME signals generated by the second or third macroscopic fracture event tend to have smaller amplitudes, and given some random influences on the amplitudes (like slightly asymmetric fracture and therefore slightly different source-sensor distances), we did not test enough samples to verify a direct crack length to amplitude correlation. No preferred polarisation direction was observable. Compared to PEEK and PP, the amplitudes of the EME signals emitted by the fracture of the PTFE specimens are at least one order of magnitude smaller.

4.1.4 RTM6

For the epoxy resin RTM6 only brittle fracture is observed, starting directly at the notch tip. As for PTFE, the crack stops after a certain crack length L_1 (see Fig. 13). The length L_1 of

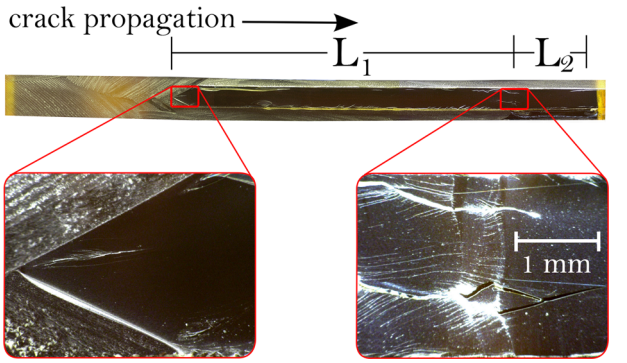

Fig. 13 Microscopy image of RTM6 specimen fracture surface. *Left* Start of brittle fracture with smooth fracture surface at notch tip. *Right* End of first and start of second macroscopic fracture event

this first fracture event is almost the full available specimen length. This first fracture emits a pair of well measurable AE and EME signals. Subsequently one or more additional macroscopic fracture events occur with much smaller crack lengths. The EME signals emitted by these events are very weak but still measurable with our set-up. The EME signals of RTM6 are the weakest of all tested polymers. The polarisation of the first rise in EME voltage signal seems to be completely random.

An evaluation of the acquired EME signal's amplitudes based solely on the mechanical and electrical properties of the polymers appears to not be practicable since the polymers also exhibit different kinds of fracture mechanisms. Other influences may be the inter- and intramolecular bonding or the chemical composition in general. In any case, additional investigation is needed.

4.1.5 Crack Propagation Velocities

For the determination of the crack velocities we assume the voltage signals at the EME sensors to rise as long as the crack surface increases (and bonds are breaking) i.e. as long as the crack propagates. Electric relaxation is neglected since it's time constants are much larger than the actual fracture times. As mentioned above, the signals are superpositions of electric signals generated by various sources. For the first signal rise we assume little influence by sensor and specimen movement. The higher frequencies attributed to crack wall vibration are assumed to be influenced by crack wall movement perpendicular to the crack propagation direction. We assume the low frequency part of the signal, considered to be generated by charge separation, to be a more reliable source for information about the crack's propagation characteristic. Therefore, for the determination of the crack velocities we applied low pass filtering to all EME signals to remove the higher frequencies generated by vibrations. The filter frequency has to be low enough to filter all frequencies higher

than the base signal but has to be high enough for the filtered signal to still adequately represent the base signal's rise characteristics. For RTM6 and PTFE a 5 kHz low pass filter (butterworth, 6th order) proved adequate (see Fig. 14, top), while for the steeper rises of the PP and PEEK signals a higher cutoff frequency was needed (12 and 15 kHz, respectively, butterworth, 6th order). Furthermore, the EME signals emitted during fracture of PEEK and PP were recorded with a different set-up. For comparable results, i.e. for matching the transfer functions of both used set-ups, an additional 1 kHz high pass filter (butterworth, 1st order) was applied to all PEEK and PP EME signals. Figure 2 shows the transfer function of the PEEK/PP set-up with the applied high pass filter (light blue dots) which now matches the bandpass characteristics of the PTFE/RTM6 set-up. The additional filter only marginally influences the characteristic of the first rise of the PEEK and PP EME signals.

To determine the actual velocity profiles we use a method as is illustrated in Fig. 14. After filtering we obtain the component of the EME signals which are attributed to pure charge separation (Fig. 14, top). Under the assumption that charges are separated as long as the crack propagates we normalize the first signal rise to the maximum crack lengths as determined from post-mortem microscopy of the fracture surfaces. This results in a function for the time dependence of the crack tip position (Fig. 14, middle). The first derivative of this function then gives the time dependent crack velocity (Fig. 14, bottom). This method uses additional assumptions. We have to assume that the density of separated charges is in fact the same for every incremental crack surface area. Additionally, we have to assume that the polarisation of the net charge density does not change during the propagation of the crack. For this reason, it should be noted that this method only works with half of the recorded EME signals, i.e. those signals that show a distinct polarity. The presented result therefore only includes these signals.

For the PEEK specimens, where the crack propagates in two stages, we cannot normalize the maximum to the total crack length. For the different stages the ratio of the amplitude rises differs from the ratio of the crack lengths. This indicates a difference in surface charge density for the two stages. Therefore, the velocities were determined separately for each stage, as indicated in Fig. 15.

Table 3 summarizes the obtained maximum crack velocities v_{max} for unstable crack growth for each polymer. For comparison, the transversal sound velocities v_T and the respective rayleigh wave velocities v_R are also given. These values were calculated using Bergman's approximate [39], with the material parameters shown in Table 1. The obtained values for v_{max} vary greatly for the different polymers, while all of the velocities are below the rayleigh wave velocities which define the upper limits for the crack propagation velocities in these solids.

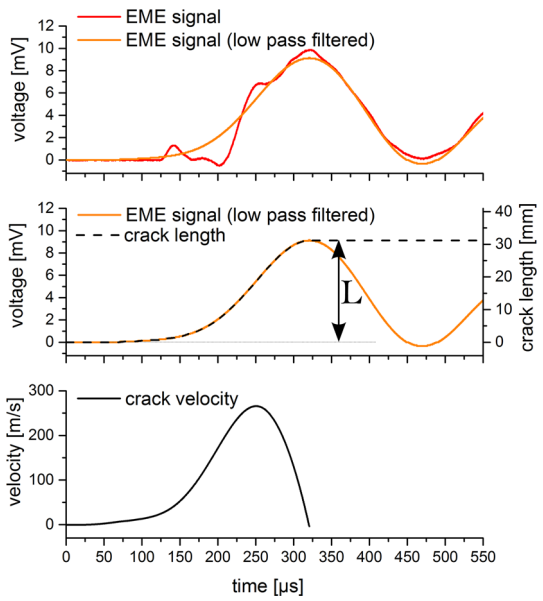

Fig. 14 Method of crack velocity determination from exemplary PTFE EME signal. *Top* application of low pass filter. *Middle* normalizing signal rise to maximum crack length as derived from post-mortem microscopy. *Bottom* velocity as derivative of crack length

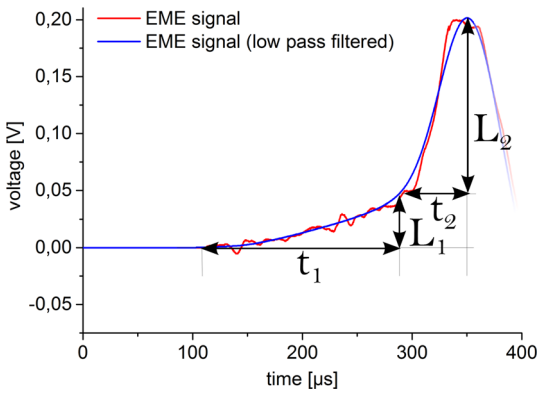

Fig. 15 Two stages of crack propagation of PEEK fracture. Normalization of crack length is carried out for each stage independently

Table 3 Transversal wave velocities, Rayleigh wave velocities and calculated maximum crack propagation velocities for the polymers used

Material	v_T (m/s)	v_R (m/s)	v_{max} (m/s)	$\sigma_{v_{max}}$ (m/s)
RTM6	983	926	466	±121
PTFE	337	321	226	±48
PP	761	720	673	±185
$PEEK_{stage1}$	982	924	210	±40
$PEEK_{stage2}$	982	924	853	±132

For PEEK, the second stage of its fracture has the highest crack propagation velocity whereas the crack propagates much slower in the first stage.

Of all the tested polymers, PTFE features the lowest value for v_R. This is reflected in the obtained crack propagation velocity.

No comparison is made to polymer crack velocities from literature since the crack propagation velocity depends on the local stress states and therefore on the specific specimen geometry as well as potentially existing residual stresses originating from the materials processing conditions. Nevertheless, the relation between the derived maximum crack velocities and the Rayleigh wave velocities indicate that the proposed approach could lead to meaningful crack velocity profiles.

The errors for the velocities given in Table 3 are the standard deviation derived from the averaging process. Additional error sources are the choice of the low pass filter frequency as well as the determination of the total crack length. Especially for the materials with partially ductile crack propagation the determination of the beginning of the EME signal generating brittle crack may prove challenging. These influences differ for the different polymers but are estimated to be of the same order as the standard deviation.

4.2 Fibre Fracture Tests

EME measurements with capacitive probes during tensile tests of fibre bundles containing a few thousand carbon fibres have been conducted before and reported in [9,40]. The EME signals emitted by failure of single fibres before the failure of the whole bundle reported in these texts are dominated by the bandwidth of the applied sensor system, i.e. all show a characteristic form of a fast exponential rise and a slow exponential decay which reflects the characteristic response of the applied sensor system to a step function in input voltage. Furthermore, all detected signals of carbon fibre fracture reported in [9,40] exhibit the same polarity.

Figure 16a shows EME and AE signals detected during the fracture of a HM type carbon fibre. The EME signal exhibits the fast rise that has been reported before. Only a small fracture of all recorded signals exhibit this kind of rise. As for the polymers we expected the rise times to correlate with the fracture times and velocities. The measured rise times are in the range of 200 ns, for all tested fibre types, which is the lower limit of our measurement equipment (3 MHz low pass filter). Figure 16b shows the response of our acquisition system to a step function (20 ns rise) generated by an arbitrary waveform generator and normalized EME signals for the three fibre types. Since all signal rises are identical to our systems step response the actual rise times cannot be determined with the current set-up and are possibly of the same order of magnitude or smaller. Considering crack propagation velocities of the order of 10^3 m/s and crack lengths in the range of a few µm the crack propagation times are expected to be in the nanosecond range. In a more detailed approach Sause et al. [32], combining AE measurements and FEM modelling of single fibre fracture, obtained a total crack duration of 1.2 ns for carbon fibres with comparable diameter. Therefore, an acquisition board with an appropriate bandwidth and sample rate is needed to measure these fast processes.

After the fast initial rise the characteristics of the EME signals varies for every recorded signal and no distinct characteristic can be assigned to a specific type of carbon fibre. This may be attributed to the nature of the fracture process. All three fibre types showed similar behaviour for this tensile test and fractured into several fragments which, caused by the released energy, moved in arbitrary directions. The charges and the movement directions, with respect to the sensor, of the fibre fragments then determine the further characteristics of the EME signals.

The majority of the recorded EME signals are of the kind that is shown in Fig. 17a. These signals do not exhibit the first sharp signal rise. Instead, the voltage signal increases much slower. A possible explanation might be that the actual fracture signal is not recorded due to the relative orientation of the fracture surfaces and the sensor and only the movement of the charged fragments contributes to the detected signal.

No specific polarity of the recorded EME signal was observed either. If there is a preferred polarity, as has been reported, it was not observed due to the additional random influences on the detected EME signals, i.e. the position of the cracks relative to the sensor and the movement of the fibre fragments.

With the intention to reduce free movement of the fibre fragments after fracture, tensile tests with fibre bundles containing less than 50 fibres were conducted for the three fibre

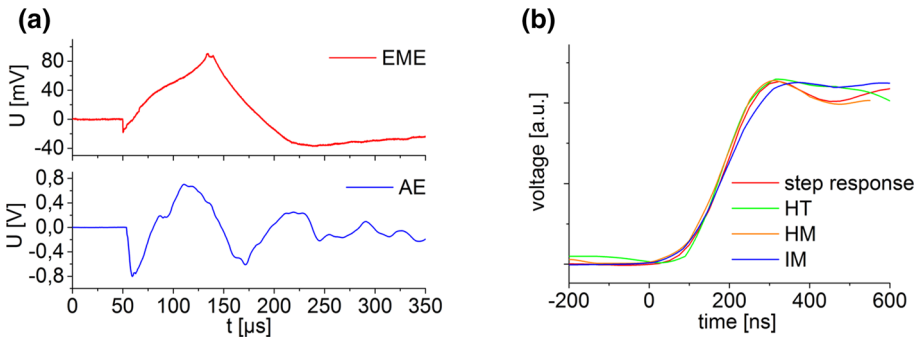

Fig. 16 **a** Exemplary EME and AE pair recorded during fracture of a HM type single carbon fibre, exhibiting step-like rise time. **b** Step type EME signals for three fibre types in comparison to the measurement system's response to step function. Normalized (Color figure online)

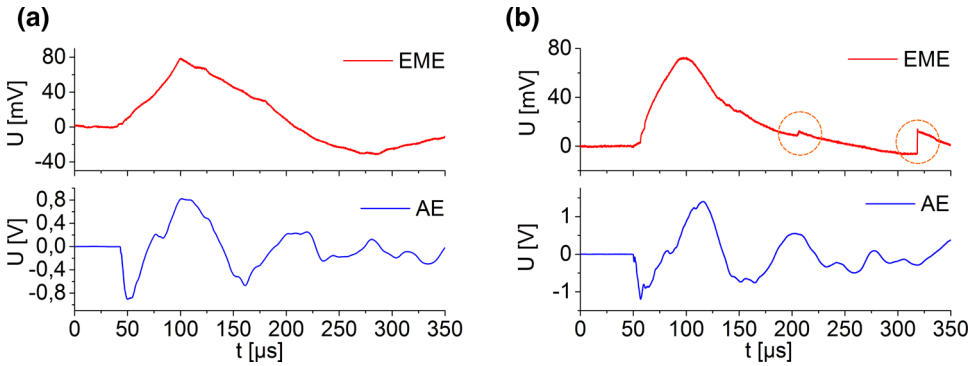

Fig. 17 **a** Exemplary EME and AE pair recorded during fracture of a HM type single carbon fibre. **b** Exemplary EME and AE pair recorded during fracture of a bundle of HM type carbon fibres. *Marked with circles* EME signatures without correlated AE signatures

types. A clear correlation between number of fibres per bundle and number of emission events could not be observed. First fibre failure occurred at about 80–90% of the maximum load. Each fibre fracture is accompanied by a small load drop in the load–displacement curves and an AE/EME signal pair (recorded in synchronized mode). The number of such fibre fractures varied between 0 and 5, with the occasional occurrence of multiple events recorded in one signal (as shown in Fig. 17b). Final failure of the bundle, accompanied by multiple emission events, generated strong AE and EME signals often resulting in saturation of both channels. Figure 17b shows an EME signal of the first fibre failures of a HM type fibre bundle. Again, as for the single fibre tests, the two different kind of signals could be observed. Here, the signals with the rapid rise could be observed more often. Due to the restriction of movement of the fragments within the fibre bundle, these signals now also exhibit the slow exponential decay that is attributed to the 1 kHz high pass filter of the measurement system.

A distinction of the fibre types by the analyses of the EME signals could not be made, due to a limitation of the acquisition board and the significant influence of the dynamics of the fibre fragments. Nevertheless, relatively strong EME signals could be measured for the single fibre and fibre bundle fracture tests which clearly differ from the EME signals emitted by fracture of the polymers. This may be caused by the different materials, source mechanisms, post fracture dynamics, crack surface dimensions and source-sensor orientations.

The AE signals (as seen in Figs. 16 and 17) all exhibit near identical characteristics, regardless of type or number of fibres breaking. Furthermore, for every type of fibre tested, emission events occurred with additional step-like signatures in the EME signals with no indication of correlated signatures in the AE signals. An example for this observation is shown in Fig. 17b, where two additional, differently pronounced EME signatures are recorded (marked in figure) with no visible correlated AE signature. Nevertheless, the combined measurement of acoustic and electric signals has proven to be a practical approach. EME signals that are accompanied by an AE signal can be attributed to fibre fracture with certainty and therefore can be distinguished from occasional spurious signals. Furthermore, the higher amplitudes of the measured AE signals make them excellent trigger signals for the EME detection.

5 Conclusion

We presented a concept of measuring low frequency electric fields in the kHz–MHz range generated by fracture of different polymer types. This concept can be extended to other solids with low or moderate conductivity (up to order of 10^{-8}–10^{-5} S/m). The EME signals contain valuable information about the electric field generating fracture processes. In particular, a derivation of the time dependent crack velocities can be done.

During fracture tests on polymers characteristic EME signals were obtained which vary distinctly for the different types of polymers tested. The initial rise characteristics of the EME signals correlate with the crack dynamics while the different amplitudes indicate other influences that determine the electrification processes. To this end, further experimental examination is required. A method to derive velocity profiles for the crack propagation was proposed. The determined maximum crack velocities mostly correlate with the rayleigh wave velocities of the materials, indicating the applicability of this approach.

Concerning the EME of carbon fibre fracture, the set-up seems also suitable to a certain degree, but has to be adjusted to allow the measurement of the crack propagation times in the nanosecond range. Nevertheless, during the fracture of carbon fibres clear EME signals could detected that significantly differ from those obtained during the polymer fracture tests.

The presented results are expected to be beneficial as a basis for the analysis of EME of carbon fibre reinforced plastics.

Furthermore, the underlying concepts present further promising applications and, in the opinion of the authors, qualify as a basis of a nondestructive testing method to study aspects of fracture processes that are inaccessible to other techniques.

Acknowledgements This research is funded by the DFG as part of the project "Relation of electromagnetic and acoustic emission to temporal and spatial crack motion on a microscopic scale in polymers and carbon fibres".

References

1. Yamada, I., Masuda, K., Mizutani, H.: Electromagnetic and acoustic emission associated with rock fracture. Phys. Earth Planet. Int. **57**, 157–168 (1989)
2. Frid, V., Rabinovitch, A., Bahat, D.: Fracture induced electromagnetic radiation. J. Phys. D **36**, 1620–1628 (2003)
3. Misra, A., Prasad, R.C., Chauhan, V.S., Srilakshmi, B.: A theoretical model for the electromagnetic radiation emission during plastic deformation and crack propagation in metallic materials. Int. J. Fract. **145**, 99–121 (2007)
4. Hadjicontis, V., Mavromatou, C., Antsygina, T.N., Chishko, K.A.: Mechanism of electromagnetic emission in plastically deformed ionic crystals. Phys. Rev. B **76**, 5953 (2007)
5. Rabinovitch, A., Shay, A., Liraz, R., Frid, V., Bahat, D.: Electromagnetic radiation emitted during friction process. Int. J. Fract. **131**, 21–27 (2005)
6. Tsutsumi, A., Shirai, N.: Electromagnetic signals associated with stickslip of quartz-free rocks. Tectonophysics **450**, 79–84 (2008)
7. Dickinson, J.T.: Fracto-emission: The role of charge separation. J. Vac. Sci. Technol. A **2**, 1112–1116 (1984)
8. Shiota, T., Yasuda, K.: Simultaneous measurement of the emission of photons and charged particles during fracture of brittle materials. Mater. Sci. Eng. **173**, 248–52 (2010)
9. Sklarczyk, C., Winkler, S., Thielicke, B.: Die elektrische Emission beim Versagen von Faserverbundwerkstoffen und ihren Komponenten. Mat.-wiss. u. Werkstofftech. **27**, 559–566 (1996)
10. Aman, S., Aman, A., Tomas, J.: Method of crack formation analysis based on mechanoluminecence. Mater. Sci. Appl. **3**, 739–744 (2012)
11. Petrenko, V.F.: Electromechanical phenomena in ice. CRREL Special Report 96-2 (1996)
12. Koktavy, P., Pavelka, J., Sikula, J.: Characterization of acoustic and electromagnetic emission sources. Meas. Sci. Technol. **15**, 973–977 (2004)
13. Ivanov, V.V., Egorov, P.V., Kolpakova, L.A., Pimonov, A.G.: Crack dynamics and electromagnetic emission by loaded rock masses. Sov. Min. Sci. **24**, 157–168 (1988)
14. Koktavy, P.: Experimental study of electromagnetic emission signals generated by crack generation in composite materials. Meas. Sci. Technol. **20**, 015704 (2009)
15. Sedlak, P., Sikula, J., Lokajicek, T., Mori, Y.: Acoustic and electromagnetic emission as a tool for crack localization. Meas. Sci. Technol. **19**, 045701 (2008)
16. Ogawa, T., Oike, K., Miura, T.: Electromagnetic radiations from rocks. J. Geophys. Res. **90**, 6245–6249 (1985)
17. O'Keefe, S.G., Thiel, D.V.: A mechanism for the production of electromagnetic radiation during the fracture of brittle materials. Phys. Earth Planet. Int. **89**, 127–135 (1995)
18. Gade, S.O., Weiss, U., Peter, M.A., Sause, M.G.R.: Relation of electromagnetic emission and crack dynamics in epoxy resin materials. J. Nondestruct. Eval. **33**, 711–723 (2014)
19. Sause, M.G.R.: In-Situ Monitoring of Fiber-Reinforced Composites. Springer-International, Cham (2016)
20. Rabinovitch, A., Frid, V., Bahat, D.: Surface oscillations—a possible source of fracture induced electromagnetic radiation. Tectonophysics **431**, 15–21 (2007)
21. Lacidogna, G., Carpinteri, A., Manuello, A., Durin, G., Schiavi, A., Niccolini, G., Agosto, A.: Acoustic and electromagnetic emissions as precursor phenomena in failure processes. Strain **47**, 144–152 (2010)
22. Laptukhov, A.I.: Generation of an electromagnetic field during rupture of a dielectric. Russian Phys. J. **38**, 15–19 (1995)
23. Allison, F.E.: Shock-induced polarization in plastics. I. Theory. J. Appl. Phys. **36**, 2111–2113 (1965)
24. Mastrogiannis, D., Antsygina, T.N., Chishko, K.A., Mavromatou, C., Hadjicontis, V.: Relationship between electromagnetic and acoustic emissions in deformed piezoelectric media: microcracking signals. Int. J. Solids Struct. **56–57**, 118–125 (2015)
25. Takeuchi, A., Nagahama, H.: Electric dipoles perpendicular to a stick-slip plane. Phys. Earth Planet Int. **155**, 208–218 (2006)
26. Larsson, J.: Electromagnetics from a quasistatic perspective. Am. J. Phys. **75**, 230–9 (2007)
27. Haus, H.A., Melcher, J.R.: Electromagnetic Fields and Energy. Prentice Hall, Englewood Cliffs (1989)
28. Dirks, H.K.: Quasi-stationary fields for microelectronic applications. Electr. Eng. **79**, 145–155 (1996)
29. Partridge, R.E.: Capacitive probe E-field sensors. Sensor Simul. Notes **11** (1965). http://ece-research.unm.edu/summa/notes/SSN/note11
30. Baum, C., Breen, E., Giles, J., O'Nelll, J., Sower, G.: Sensors for electromagnetic pulse measurements both inside and away from nuclear source regions. IEEE Trans. Electromagn. Compat. **26**, 22–35 (1978)
31. Winkler, S.: Tear detector for mechanical loading test sample—uses capacitive sensor coupled via impedance converter to electronic evaluation circuit. DE Patent 4,004,171, C2, 1993
32. Sause, M.G.R., Richler, S.: Finite element modelling of cracks as acoustic emission sources. J. Nondestruct. Eval. **34**, 1–13 (2015)
33. Sause, M.G.R., Hamstad, M.A., Horn, S.: Finite element modelling of conical acoustic emission sensors and corresponding experiments. Sensors Actuators A **184**, 64–71 (2012)
34. Zelenyak, A.M., Sause, M.G.R., Hamstad, M.A.: Modeling of acoustic emission signal propagation in waveguides. Sensors **15**, 11805–11822 (2015)
35. Shiwa, M., Inaba, S., Carpenter, S.H., Kishi, T.: Development of high-sensitivity and low-noise integrated acoustic emission sensor. Mater. Eval. **50**, 868–874 (1992)
36. din en iso 527-1: determination of tensile properties of plastics—part 1: general principles (2012)
37. DIN EN ISO 527-2: Determination of tensile properties of plastics—part 2: test conditions for moulding and extrusion plastics (2012)
38. Koizumi, N., Yano, S., Tsuji, F.: Dielectric properties of polytetrafluoroethylene and tetrafluoroethylene-hexafluoropropylene copolymer. J. Polym. Sci. C **23**, 499–508 (1968)
39. Bergman, R.H., Shahbender, R.A.: Effect of statically applied stresses on the velocity of propagation of ultrasonic waves. J. Appl. Phys. **29**, 1736–1738 (1958)
40. Winkler, S.R.: Field emissions caused by fracture and yielding. Int. J. Fract. **136**, 221–235 (2005)